JOURNAL OF THERMOPHYSICS AND HEAT TRANSFER
Vol. 7, No. 3, July–Sept. 1993

Computational Study of Coolant Flow of Liquid Hydrogen Through an Externally Heated Duct

Robert G. Carlisle* and Houston G. Wood III†
University of Virginia, Charlottesville, Virginia 22903

The computational modeling of the two-dimensional flow of liquid hydrogen coolant within the leading edge of the National Aero-Space Plane (NASP) engine structure is described. The model includes consideration of the effects of the variable thermophysical properties of hydrogen, axial conduction within the leading-edge material, and the coupling of the energy and momentum equations in the flow. The reduced Navier-Stokes equations are solved by parabolic marching of the discretized finite difference equations down the coolant passage. The importance of the consideration of the above factors was demonstrated as the calculated temperatures agreed with those predicted by earlier empirical methods for moderate heat transfers, but differed for the heat transfer magnitudes of interest. The form of the expression of the solid/fluid interface condition was found to be an important factor in determining the accuracy and speed of convergence of the algorithm. The ability of the hydrogen coolant system to cool the incident heat load was found to be marginal: moderately increased incident heat loads would exceed the capabilities of the modeled system. Parametric studies were done to show the relative importance of the temperature, pressure, and velocity of the coolant fluid on the cooling capabilities of the system.

Nomenclature

A = vector operator in Eq. (10)
a = velocity of sound
C_i = vector constants in Eq. (12)
c_p = specific heat at constant pressure
c_v = specific heat at constant volume
D = duct height
h = heat transfer coefficient
i = index
k = thermal conductivity
L = typical dimensional distance (duct height)
l = mixing length
M = Mach number
Nu = Nusselt number
Pr = Prandtl number
p = pressure
q = heat transfer rate
Re = Reynolds number
S_p = pressure gradient vector
T = temperature
U = bulk fluid velocity
u = streamwise velocity
u_s = boundary-layer edge velocity
u_t = friction velocity
v = cross-stream velocity
x = streamwise ordinate
y = cross-stream ordinate
γ = ratio of specific heats
ε_h = turbulent thermal diffusivity
ε_m = turbulent momentum diffusivity
Θ = velocity and temperature vector in Eq. (10)
μ = dynamic viscosity
ν = kinematic viscosity
ρ = density

Subscripts
b = in bulk of fluid
c = cross stream
cl = centerline
e = in exit plane
m = in metal/solid region
mf = at solid/fluid interface
$m1$ = one node into solid from solid/fluid interface
p = on previous plane in iteration procedure
w = at wall
∞ = entrance plane conditions

Superscript
$'$ = dimensional quantity

I. Introduction

IN this article, we describe a computational model developed to calculate the heat transfer across an externally heated solid boundary into a fluid with variable transport properties. The variation of the fluid properties with the fluid temperature and the coupling of the temperature distribution of the solid boundary with the temperature distribution in the fluid are complicating factors. In the application under consideration, liquid hydrogen is used to cool a massively heated structure. Failure to account for these complicating factors could lead to erroneous conclusions regarding the ability of the liquid hydrogen coolant passages to sufficiently cool the surrounding structure.

The physical problem that is computationally modeled is the proposed flow of liquid hydrogen coolant through the engine cowl lip of the National Aero-Space Plane (NASP). Under certain conceived flight conditions, the structure of the airflow on the underside of the NASP will cause the shock wave anchored to the leading edge of the main structure to impinge on the bow shock wave on the engine cowl lip. This type of shock interaction has been observed to cause severe local increases in aerodynamic heating.[1,2] The surface heating rates of some forms of shock interaction are estimated[3,4] at 600 MW/m^2, (50,000 Btu/ft^2-s). This heating rate is extremely massive, larger than heating rates estimated for solar probes.[5] However, the thickness of the shock effects are dependent on the leading-edge radius and is likely to be a fraction of a millimeter.

Received Aug. 3, 1991; revision received Sept. 21, 1992; accepted for publication Sept. 22, 1992.

*Graduate Research Assistant, Department of Mechanical and Aerospace Engineering. Member AIAA.
†Associate Professor, Department of Mechanical and Aerospace Engineering. Member AIAA.

Edney[6] described six kinds of shock interference patterns. The severest thermal loads, described above, are caused by type IV interference. It is characterized by the impingement of a supersonic jet, created at the position where the shocks interact, on the underlying structure.

Several options exist for mitigating this massive heat load. Among these are ablative shields, transpirative cooling, and internal cooling. The focus of this work is on internal tangential cooling by liquid hydrogen. Other coolant fluids are under consideration, principally, liquid sodium and to a lesser extent, water. Of the coolant fluids under consideration, liquid hydrogen has the singular advantage of also being intended as the fuel for the NASP's SCRAMjet. Function as a coolant may also provide necessary preheating of the fuel prior to combustion in the engine. The principal objections to using liquid hydrogen as a coolant are that the heat capacity of the liquid is low compared to alternate coolants, and that the flow past the heated portion of the structure may be inefficient in the removal of heat from the structure because the hydrogen may be locally vaporized. Accurate modeling of this internal flow will aid in assessing the heat transfer capabilities of such a system.

Scotti[3] has performed a similar analysis, assuming constant fluid bulk properties. He compared the cooling efficiencies of three prospective coolants: 1) liquid hydrogen, 2) liquid sodium, and 3) water, in the NASP coolant panel application. He concluded that for turbulent flows all three coolants are feasible or near feasible. Several empirical formulas have been proposed for calculation of heat transfer coefficients in turbulent flows of liquid hydrogen. Dziedzic et al.[7] analyzed hydrogen cooling in a cooling panel and demonstrated the variations in calculated panel performance when the calculations were based on different correlations for heat transfer coefficient. They compared results obtained using these correlations with results obtained from using the commercial fluid dynamics code FLUENT. They found some agreement between one of the correlations and the CFD code for cases in which a constant heat flux was applied. However, they did not find detailed agreement for cases in which they applied a massive localized heat load.

The most complex of these correlations, that with which Dziedzic et al.[7] found the greatest agreement, was by Taylor.[8] It is of the form

$$Nu_b = 0.023 Re_b^{0.8} Pr_b^{0.4} (T_w/T_b)^{-0.57-1.59(D/x)} \tag{1}$$

It is intended to model both entrance effects and the effect of variable properties. This correlation and others like it were found by identifying the best fit with the extensive available experimental data. For hydrogen well away from the critical point, Taylor found that 87% of the experimental data available for the heat transfer coefficient deviated less than 20% from values calculated from Eq. (1). However, for hydrogen at pressures less than 3.6 MPa and inlet temperatures less than the critical temperature, only 40% of the data were within these limits.

None of the experimental data involved large spatial differences in heat transfer rate. Like the correlations of previous researchers, Eq. (1) is dependent on the assumption of similarity of the developing boundary layer. It assumes that the relationship between the nondimensional quantities are not affected by flow history or large local changes in heat transfer rate. Thus, the similarity requirement cannot be assumed in a flow region in which the boundary conditions have a strong dependence on position, such as close to the region of massive heat flux. The "spikes" in heat transfer coefficient observed by Dziedzic et al.[7] probably resulted from the fact that the form of the heat transfer coefficient does not incorporate effects of spatial changes in the shape of the boundary-layer temperature profile.

The present work solves the parabolized Navier-Stokes (PNS) equations for flows of liquid hydrogen, with temperature-dependent thermophysical properties, through a heated channel. The temperature distribution within the solid forming the boundary of the fluid is fully coupled with the temperature distribution within the fluid, and the massive heat transfer is applied on the external (nonhydrogen) face of the solid. Use of the PNS equations to solve for flows through ducts is a well-established technique. While it is common, even necessary, to iterate on each cross-stream plane of the flow to calculate the fluid pressure, some other works have, as this work does, iterated other coupled equations. Buelow et al.[9] iterated the chemistry on each plane to model supersonic/hypersonic flows in chemical equilibrium. Several researchers iterated relationships for turbulence parameters to couple the fluid turbulence,[9,10] though this calculation is often spatially lagged because convergence of the fully coupled method can prove difficult. The coupling of the thermal distribution in a solid with that in a convective boundary layer has been examined recently by Guedes et al.[11] for laminar flows.

II. Computational Methodology

The flow is modeled through a two-dimensional, straight domain, as shown in Fig. 1. A portion of the domain (cross-hatched) is considered to be of a solid material whose thermal properties and physical boundaries are fixed. The remainder of the domain, between the solid and the "upper" boundary, contains the fluid for which the thermal properties are temperature and pressure dependent. It will generally be assumed that although the pressure varies within the fluid, this variation is small compared to the inlet pressure. With this assumption, the fluid properties are calculated for the local temperature and the inlet pressure. The pressure variations have been calculated by the model, and these calculations support the assumption that the pressure variation is small compared to the inlet pressure.

A. Governing Equations

The equations to be solved in the domain are the equations expressing conservation of mass, momentum, and energy. Expressed in a parabolized form these are

$$\frac{\partial}{\partial x}(\rho u) + \frac{\partial}{\partial y}(\rho v) = 0 \tag{2}$$

$$\rho u \frac{\partial u}{\partial x} + \rho v \frac{\partial u}{\partial y} + \frac{\partial p}{\partial x} = \frac{1}{Re}\frac{\partial}{\partial y}\left(\mu \frac{\partial u}{\partial y}\right) \tag{3}$$

$$\rho u \frac{\partial v}{\partial x} + \rho v \frac{\partial v}{\partial y} + \frac{\partial p}{\partial y} = \frac{1}{Re}\left[\frac{4}{3}\frac{\partial}{\partial y}\left(\mu \frac{\partial v}{\partial y}\right) + \frac{\mu}{3}\frac{\partial^2 u}{\partial x \partial y}\right] \tag{4}$$

$$\rho c_p \left(u \frac{\partial T}{\partial x} + v \frac{\partial T}{\partial y}\right) - (\gamma - 1)M_\infty^2 \left(u \frac{\partial p}{\partial x} + v \frac{\partial p}{\partial y}\right) = \frac{1}{PrRe}\frac{\partial}{\partial y}\left(k \frac{\partial T}{\partial y}\right) + \frac{(\gamma - 1)M_\infty^2}{Re}\mu \left(\frac{\partial u}{\partial y}\right)^2 \tag{5}$$

here μ and k include both the thermodynamic quantities of turbulence and a contribution from turbulence models calculated by the mixing length model described by Cebeci and Bradshaw.[12]

All the quantities above have been nondimensionalized against the inlet duct height L and the conditions of the fluid at the inlet, i.e.

$$u = \frac{u'}{U_\infty} \quad v = \frac{v'}{U_\infty} \quad x = \frac{x'}{L} \quad y = \frac{y'}{L}$$

$$T = \frac{T'}{T_\infty} \quad p = \frac{p'}{\rho_\infty U_\infty^2}$$

$$\rho = \frac{\rho'}{\rho_\infty} \quad \mu = \frac{\mu'}{\mu_\infty} \quad k = \frac{k'}{k_\infty} \quad c_p = \frac{c_p'}{c_{p\infty}} \tag{6}$$

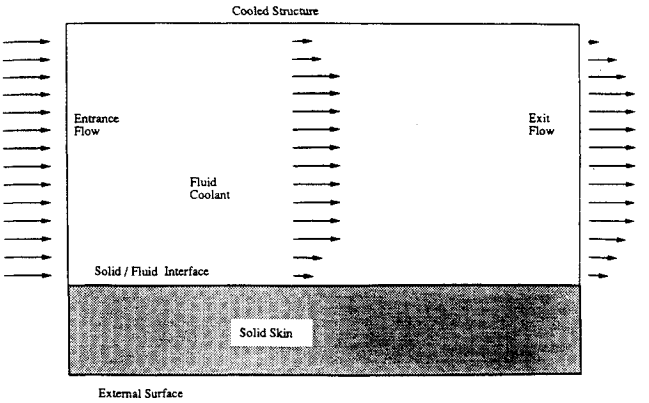

Fig. 1 Computational domain: solid region shaded.

and the following nondimensional parameters are introduced:

$$Re = \frac{\rho_\infty U_\infty L}{\mu_\infty} \quad Pr = \frac{\mu_\infty c_{p\infty}}{k_\infty} \quad M_\infty = \frac{U_\infty}{a_\infty} \quad \gamma = \frac{c_{p\infty}}{c_{v\infty}} \tag{7}$$

These reduced Navier-Stokes (RNS) equations are reached from the full equations of motion by making the general assumption that the streamwise velocity of the flow is much greater than the cross-stream velocities. Because of this, the streamwise viscous terms of the full Navier-Stokes equations can be omitted. This is a more complete system of equations than the boundary-layer equations, because it allows the boundary layers to grow to a size comparable to the typical length scale of the flow (here L).

This set of equations is still elliptic in the pressure terms. An assumption that the pressure gradients in the streamwise direction are much greater than those in the cross-stream direction allows the decoupling of these terms. Thus, the pressure has one component p_{cl} which varies only in the streamwise direction, and another component p_c which varies only in the cross-stream direction, i.e.

$$p = p_{cl} + p_c \tag{8}$$

$$\nabla \cdot p = \begin{bmatrix} \frac{\partial p_{cl}}{\partial x} \\ \frac{\partial p_c}{\partial y} \end{bmatrix} \tag{9}$$

With the pressure expressed this way, the equations are parabolic. Therefore, they can be solved by a single sweep through the fluid portion of the domain in the direction of the flow.

To prepare the equations to be discretized, it is simplest to write them in vector form (following the formulation presented by Fletcher[13]). The first two components of the "velocity" vector are the streamwise and cross-stream velocities, u and v, and the third component is the fluid temperature T.

So the parabolic equations can be expressed as

$$\rho u \frac{\partial \Theta}{\partial x} = A\Theta + S_p \tag{10}$$

where

$$\Theta = \begin{bmatrix} u \\ v \\ T \end{bmatrix} \quad S_p = \begin{bmatrix} -\frac{\partial p_{cl}}{\partial x} \\ -\frac{\partial p_c}{\partial y} \\ 0 \end{bmatrix} \tag{11}$$

$$A\Theta = C_1(T) \frac{\partial}{\partial y} C_2(T) \left(\frac{\partial \Theta}{\partial y} \right) - \rho(T) v \frac{\partial \Theta}{\partial y} + C_3 \left[\frac{1}{\rho} \left(-u \frac{\partial \rho}{\partial y} - \frac{\partial \rho v}{\partial y} \right) \right] + C_4 \frac{\partial}{\partial y} \left[C_5(u, T) \frac{\partial \Theta}{\partial y} \right] \tag{12}$$

$$C_1(T) = \frac{1}{Re_\infty} \begin{bmatrix} 1 \\ \frac{4}{3} \\ [Pr_\infty c_p(T)]^{-1} \end{bmatrix} \quad C_2(T) = \begin{bmatrix} \mu(T) \\ \mu(T) \\ k(T) \end{bmatrix}$$

$$C_3 = \frac{1}{Re_\infty} \begin{bmatrix} 0 \\ 1 \\ 0 \end{bmatrix} \quad C_4 = \frac{1}{Re_\infty} \begin{bmatrix} 1 \\ 0 \\ 1 \end{bmatrix}$$

$$C_5(u, T) = \begin{bmatrix} \rho(T)\varepsilon_m(u, T) \\ 0 \\ \rho(T)\varepsilon_h(u, T) \end{bmatrix} \tag{13}$$

The turbulence model applied is the mixing length approximation developed by Cebeci and Bradshaw.[12] This has the advantages of being straightforward to program, is appropriate for some of the aspects of this application, and does not require solving for additional transport properties, as does the k-ε model. Its disadvantages are that it is based on empirical constants not necessarily accurate for flows with parameters outside the range of the empirical basis, it is not appropriate for cases when the boundaries curve, and it (and any other common model) does not account for the turbulent variations in fluid thermophysical properties.

The exposition of the governing equations to be solved is completed by the heat distribution equation in the solid portion of the domain:

$$\frac{\partial^2 T}{\partial x^2} + \frac{\partial^2 T}{\partial y^2} = 0 \tag{14}$$

B. Boundary Conditions

The boundaries of the fluid domain are the entrance, exit, and side walls of the coolant passage. At the entrance of the domain, the flow is a specified, purely streamwise, "slug" flow.

$$u(0, y) = 1 \qquad v(0, y) = 0 \tag{15}$$

The fluid boundary conditions on the walls of the coolant passage are simple no-slip, no-penetration conditions:

$$v(x, 1) = v(x, 0) = u(x, 1) = u(x, 0) = 0 \tag{16}$$

The thermal boundary conditions are that the fluid inlet temperature is specified, that there is a specified heat flux through the outer boundary (at $y = -y_0$), that the inner boundary is adiabatic, and that there is no heat flux out of the computational domain through the solid (at $x = 0$ and $x = x_e$):

$$T(0, y) = T_f \qquad 0 < y < 1 \tag{17}$$

$$q(x, -y_0) = q_w \qquad q(x, 1) = 0 \tag{18}$$

$$q(0, y) = 0 \qquad -y_0 < y < 0 \tag{19}$$

$$q(x_e, y) = 0 \qquad -y_0 < y < 0 \tag{20}$$

As with the velocity boundary conditions, the thermal condition of the fluid at the exit is not specified.

The combined fluid momentum and energy equations are solved with these boundary conditions by an iterative procedure described in Ref. 14. The parabolized equations are

solved on each cross-stream line, successively in the direction of the flow starting from the inlet plane. Once the exit plane is reached then, depending on which of the methods detailed directly below is being used to couple the fluid thermal equations with the solid equations, either the entire marching process is restarted after the application of the thermal boundary conditions on the solid portion of the exit plane, or the thermal equations are solved in the solid and then the marching process is restarted through the fluid.

The internal thermal boundary between the fluid and the solid could have been treated in several iterative ways. It was found that sweeping the entire computational domain in the flow direction at the same time was extremely slow to converge. It was also found that passing an interface temperature distribution based on thermal/fluid calculations to the solid region and returning an interface heat transfer distribution based on thermal calculations in the solid region to the fluid calculations was prone to spatial numerical instabilities.

The preferred treatment of the interface condition was similar to the previous one, except that different quantities are passed between the fluid and the solid solvers. The fluid equations are solved based on specified temperatures along the solid/fluid interface. Then the thermal equations are solved in the solid based on local heat transfer coefficients calculated from the temperature gradients predicted in the fluid solutions. The solid solution then passes the interface temperatures to the fluid solver and the cycle continues. The condition can be expressed as

$$q(x) = h(x)(T_{mf} - T_\infty) \tag{21}$$

where $q(x)$ is the heat transfer from the solid to the fluid, $h(x)$ is the calculated heat transfer coefficient, T_{mf} is the temperature at the nodes on the fluid/solid boundary, and T_∞ is the freestream fluid temperature. Discretizing this in terms of the fluid nodal temperatures, it becomes

$$[(T_{m1} - T_{mf})/\Delta y_m] = h(x)(T_{mf} - T_\infty) \tag{22}$$

or

$$T_{mf}[\Delta y_m h(x) + 1] - T_{m1} = \Delta y_m h(x) T_\infty \tag{23}$$

This last form can be incorporated into the matrix form of the Laplace equation and can be adjusted so that the matrix is symmetric. This method, with suitable damping, converged swiftly to average relative errors between iterations of less than 0.1 K, after only 20 iterations.

C. Fluid Properties

With the assumption that changes in the pressure of the fluid are small compared to the fluid pressure, the density, viscosity, specific heat capacity, and thermal conductivity of hydrogen are all continuous functions of the fluid temperature. The additional assumption is also made that the pressure is above the fluid's critical pressure. In this case, there is no possibility of entering a two-phase region which would require the treatment of the mechanics of hydrogen boiling. The critical pressure of hydrogen is ≈1.3 MPa (13 atm), well below the pressures under consideration.

The tabulated properties of liquid/gaseous hydrogen are available for temperatures up to the onset of dissociation at about 3000 K (McCarty et al.[15]). The fluid temperature could be recalculated at each node in the computational domain by including one of several public domain programs for hydrogen fluid properties, based on temperature and pressure or by calculating fluid properties from a look-up table. However, for speed of calculation, the properties were expressed in terms of polynomials, matched to the experimental/analytical property values over a large range of temperatures. This was the method used because it was surprisingly fast and was found to vectorize excellently.

D. Variable Grid

Several researchers have noted the difficulty in modeling the heat transfer from a solid boundary into a liquid.[16] Since the heat transfer is a first derivative of the calculated temperature, greater computational accuracy is necessary to find the heat transfer accurately, or in cases such as this, to find accurate temperature when the heat transfer is not known and is critical to the calculation. To accurately find the gradients of a quantity, it is necessary to refine the grid in areas where the gradient is large, following the principle suggested by Thompson et al.[17] So rather than refining the grid over the entire computational region, the approach is taken to refine the region in the fluid near to the solid boundary, where the temperature gradients are known to be largest. Since it is also known that these gradients will be normal to the solid boundary, it is only in this direction that the grid needs to be refined. The grid is maintained as a rectangular grid with each streamwise step a constant size and each cross-stream grid layout equal, because that is required in the parabolic expression of the governing equations.

The grid can either be made very small in refined regions and large elsewhere, or it can be made to vary smoothly from the finest to the coarsest region. The latter approach was chosen because it avoids the existence of an artificial boundary in the fluid where there is a coarse grid on one side and a fine grid on the other. The equations would have to be discretized to a higher order of accuracy for the nodes on this boundary, which would destroy the symmetry of the solution method. The grid is made to vary geometrically, each grid spacing out from the solid boundary in the cross-stream direction is a constant percentage larger than its neighbor. As this percentage is kept small (i.e., between 0.01–0.1), the method is generally stable and only small modifications to the difference equations are necessary to ensure local conservation of mass and energy.

The grid spacing in the streamwise or x direction need not be made fine for accurate predictions of temperature and heat transfer. However, as the variation in the y direction is small close to the solid/fluid boundary, the grid has a very large aspect ratio in this region. There is a limit on how large this ratio can be for stable computations. In general, the x direction spacing is close to the average spacing in the y direction, and the grid aspect ratio close to the wall is less than 30.

E. Convergence

Different degrees of convergence were required of the different iterative processes. To ensure conservation of mass in the fluid in the calculation of pressure gradient, the mass deficit was required to be less than 10^{-7} of the total. The maximum normalized change in fluid temperature or fluid velocity between fluid temperature/fluid property iterations was 10^{-5}. The maximum normalized residual in the thermal calculations in the solid was 10^{-6}. In general, between overall iterations between the thermal conditions in the solid and the fluid calculations, it was only required that the maximum change in interface temperature was less than 0.05 K; however, it was confirmed in several tests that these temperatures would not change by more than 0.5 K if this requirement was increased to 0.001 K. This convergence is demonstrated in Fig. 2. For all subsequent iterations (tested to 200) after the 25th, the temperatures would coincide with those shown. The comparatively slow rise to these temperatures is due to damping applied to maintain the stability of the iterative process.

Spatial convergence of the results with the computational grid was confirmed by successively doubling the number of grid lines in the x and y directions until there was no change in interface temperatures of more than 0.1 K, or change in interface heat transfer coefficients of a similar comparative magnitude (0.01%). It was also confirmed that increasing or slightly decreasing the ratio of adjacent cross-stream grid spacings (a constant in the calculations) had a similarly small effect. Large increases in this ratio introduced numerical insta-

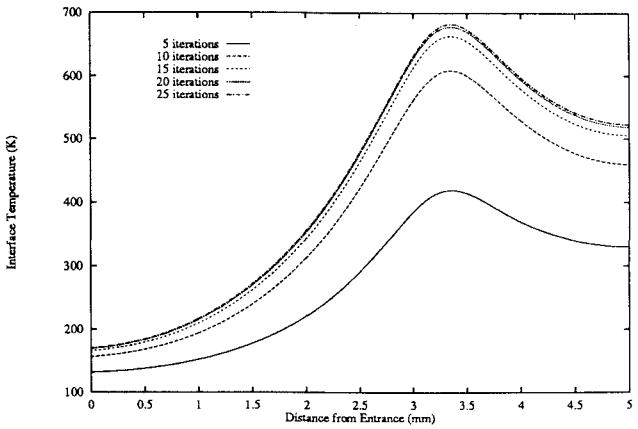

Fig. 2 Interface temperatures for successive iterations between solid and fluid thermal solutions.

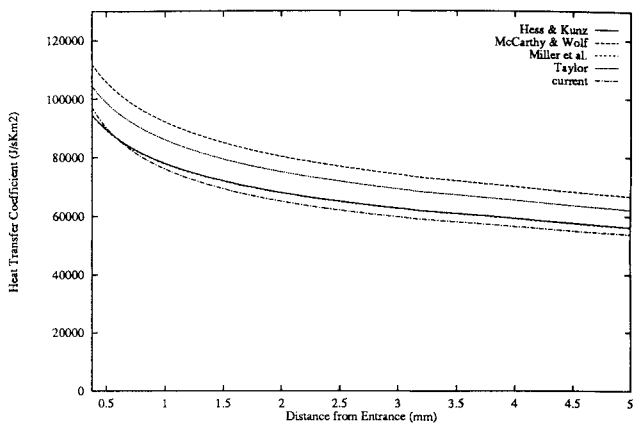

Fig. 3 Heat transfer coefficient calculated by the named correlations or by the current CFD method. Boundary temperature 190 K, fluid temperature 185 K.

bilities. Large decreases would cause less refinement of the fluid grid at the interface and lose the spatial convergence. The results presented were based on 200 cross-stream grid points in the fluid, 2000 streamwise grid points, a cross-stream grid spacing ratio of 1.03, and 30 cross-stream grid points in the solid. The finest grid spacing in the cross-stream direction was 82 nm, and the spacing in the streamwise direction was 2500 nm, for a maximum grid aspect ratio of 30.

III. Results

The algorithm described in the previous section was implemented. The input data can be varied to model a variety of situations. The most interesting are those which model heat transfers of magnitude comparable to those which might exist on the NASP cowl lip. But other cases were also run to model heat transfers of a much lower, or even zero, magnitude, to confirm that the modeling of the flow under these simple conditions was in good agreement with established results.

A. Validation

There does not exist a wide range of experimental data applicable to the cooling of a heated surface by liquid hydrogen. Therefore, the action of the algorithm developed will be compared to the empirical correlations quoted by Dziedzic et al.[7] These were developed as a best fit to data extracted from a variety of thermal and physical experimental geometries, e.g., some for constant temperature plates and some for uniformly heated ducts. As described in Sec. I, the goodness of fit of the correlations was not large. Therefore, validation with respect to these correlations is desirable, but small deviations for normal conditions are expected, and large deviations from predicted values are to be expected when the thermal environment is outside the range of application of the correlations. These correlations were suggested by Hess and Kunz,[18] McCarthy and Wolf,[19] Miller et al.,[20] and Taylor.[8] The thermal condition modeled will be that of a constant temperature semi-infinite flat plate in a cooler flow. The empirical relations are not expected to be accurate close to the leading edge (except possibly that of Taylor) and are limited in the temperature difference they can be expected to model. Figure 3 shows the variation of heat transfer coefficient with distance from the leading edge for the four correlations and the two-dimensional code. The Reynolds numbers used by the correlations are based on the distance from the leading edge of the plate and either the temperature of the plate, the temperature of the fluid, or the appropriate intermediate temperature. It can be seen that for this small temperature difference (5 K), all the correlations and the results of the two-dimensional code are in good agreement. When a larger temperature difference (50 K) is applied, there is still an agreement (shown in Fig. 4), but in this case, as in the case of extremely large temperature difference (Fig. 5), the calculations are in closest agreement with the correlation of Taylor. For smaller temperature differences, the agreement is shown best with the correlations of both Hess and Kunz[18] and Miller et al.,[20] who based the correlations on reference temperatures.

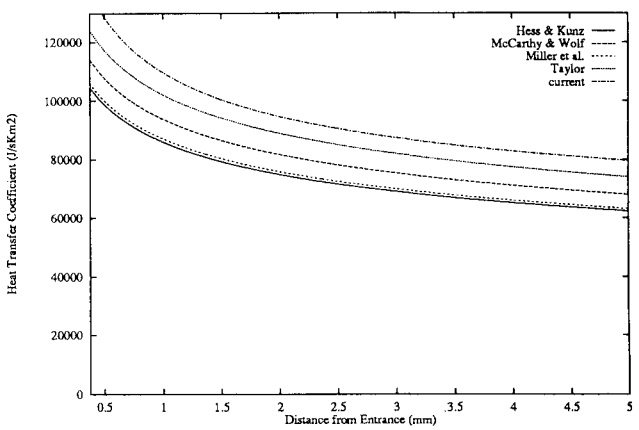

Fig. 4 Heat transfer coefficient calculated by the named correlations or by the current CFD method. Boundary temperature 190 K, fluid temperature 140 K.

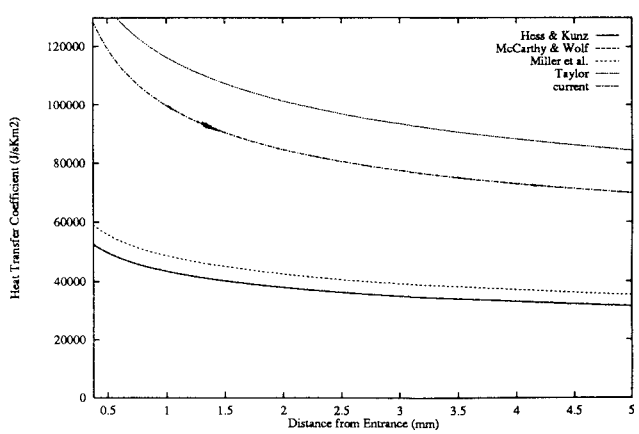

Fig. 5 Heat transfer coefficient calculated by the named correlations or by the current CFD method. Boundary temperature 700 K, fluid temperature 100 K.

B. Modeling Results

The parameters of interest in the modeled flow are 1) the magnitude of the maximum heat transfer rate; 2) the width of the heat transfer peak; 3) the fluid inlet velocity; 4) the

inlet temperature of the fluid; 5) the fluid inlet pressure; 6) the duct height; 7) the placement of the heat transfer peak relative to the duct entrance; 8) the solid skin thickness; and 9) the solid skin material.

Not all of these parameters will be fully explored in this article. The material of the skin will be taken to have the thermal conductivity of copper. Though this would not be expected to be of importance in a steady-state conduction problem, the thermal conductivity does affect the convective boundary condition, and therefore is a factor in this configuration, but the effects of its variation are not explored in this article.

The baseline parameter configuration is:

Maximum heat transfer rate	500 MJ/m^{2}s
Width of heat transfer peak	0.25 mm
Fluid inlet velocity	100 m/s
Fluid inlet temperature	55 K
Fluid inlet pressure	20 MPa
Duct height	1 mm
Peak placement (center)	3.25 mm from inlet
Solid thickness	0.5 mm
Solid thermal conductivity	469 J/ms K

These parameters are not intended to duplicate exactly the configurations appropriate to the NASP, but to produce results representative of the kind of behavior expected.

The temperature contours produced for this baseline set of parameters is shown in Fig. 6. The lower portion of the domain, -0.5 mm $< y < 0$, is the solid part of the domain, and $y > 0$ is the fluid. The extreme bunching of the contours on the fluid/solid boundary shows that the majority of the temperature drop from the external surface to the bulk of the coolant occurs in the thermal boundary layer. Figure 7 expands this region to show the heating and subsequent cooling of the fluid as it passes over the region of most intense heat flux. The cooling occurs as a result of the mixing of the heated flow with the bulk of the fluid, which occurs downstream of the region of most intense heat flux.

For this baseline configuration, the resulting temperatures along the internal (liquid hydrogen side) and external surfaces are shown in Fig. 8. The temperatures predicted here are comparatively mild, partly because of the "spreading" of the heat transfer through the metal: the maximum local heat transfer to the fluid is 230 MJ/m^{2}s, less than half that applied to the external face. This effect was noted by Scotti.[3] It becomes less pronounced for the fluid when the fluid temperature is higher as a result of increased heat transfer rates.

The most obviously significant factor in determining the maximum temperatures is the magnitude of the heat transfer input. Figure 9 shows the relationship between the interface (solid/liquid hydrogen) temperature and the heat input magnitude. Doubling the heat transfer magnitude more than doubles the interface temperatures because of decreases in the spreading of the heat transfer caused by variation of the heat transfer coefficients with the different thermal conditions.

Though the massive heating of the NASP engine cowl lip is generally quoted as a heat transfer rate per unit area, Fig. 10 shows that the more important factor is the total heat transfer rate. In this case, the width of the heat transfer peak is varied while the rate per unit area is kept constant. The resulting variation of maximum temperature with total heat transfer is similar to the case when the magnitude of the heat transfer peak is varied.

Figure 11 shows the marked effect of a decreased inlet pressure on the heat transfer efficiency. For the same series of heat transfer peak widths, but a pressure of 5 MPa rather

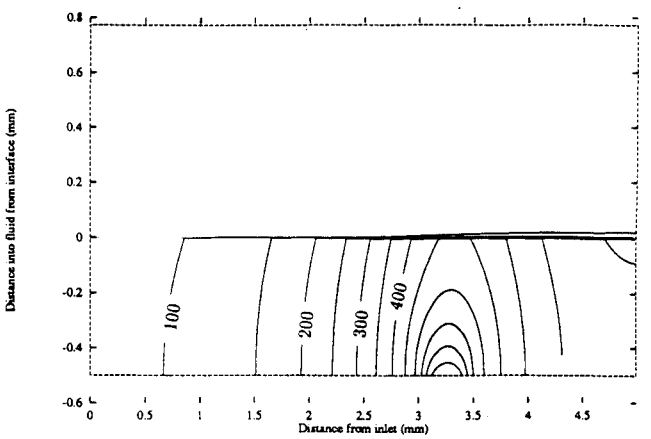

Fig. 6 Temperature contours throughout entire fluid and solid domains (50 K intervals).

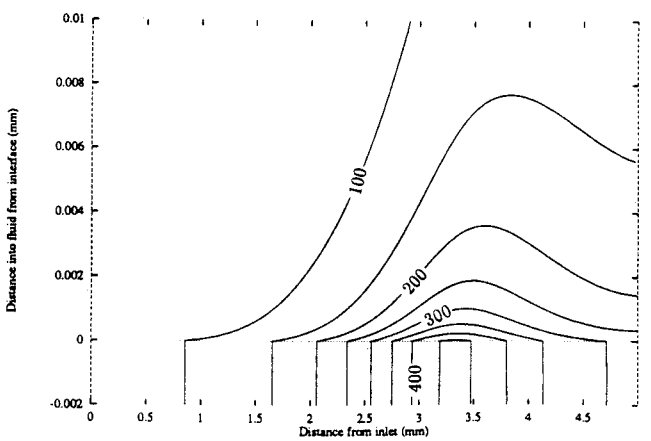

Fig. 7 Temperature contours close to fluid/solid interface (50 K intervals).

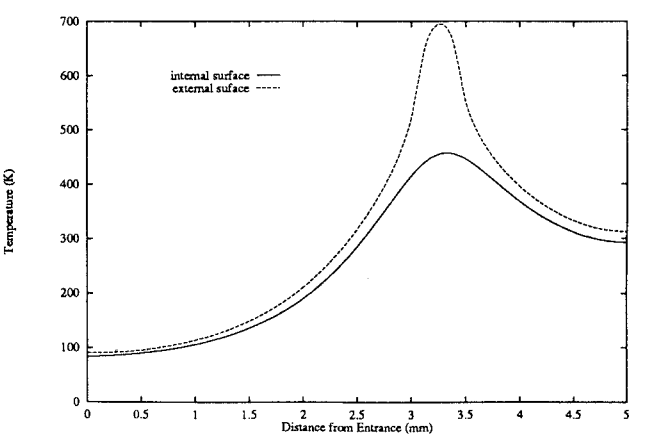

Fig. 8 Internal and external temperatures for baseline configuration.

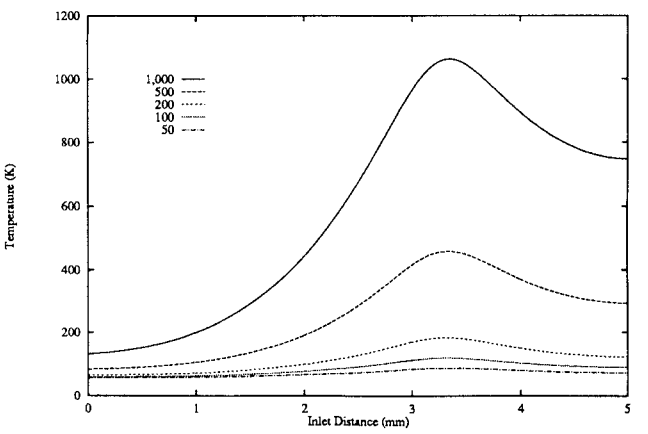

Fig. 9 Interface temperatures for a range of heat transfer rates, given in MJ/m^{2}s.

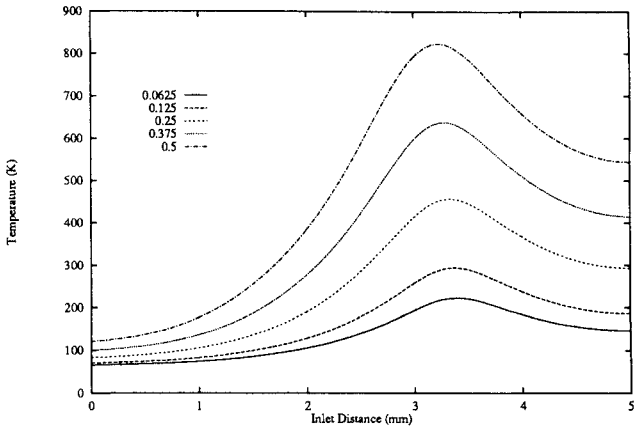

Fig. 10 Interface temperatures for a range of heat transfer peak widths, given in mm.

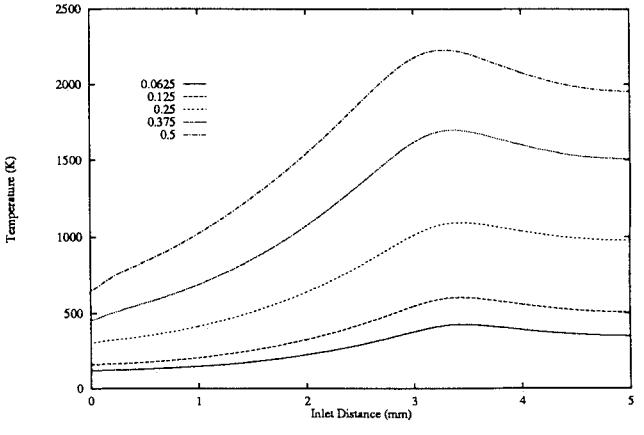

Fig. 11 Interface temperatures for a range of heat transfer peak widths, given in mm, for an inlet pressure of 5 MPa.

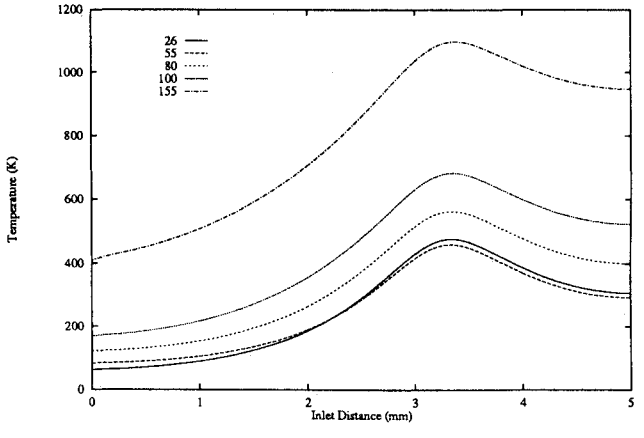

Fig. 12 Interface temperatures for a range of inlet temperatures, given in K.

than 20 MPa, this shows the solid/fluid interface temperatures resulting from a lower inlet pressure.

For the 20 MPa case, the maximum temperature reached for the widest peak (900 K for a width of 0.5 mm) is lower than that for the peak of the 1000 MJ/m²s line in Fig. 9, which corresponds to the same total heat transfer. This indicates that the cooling process is more efficient when for a diffuse heat input to the fluid a greater quantity of the coolant liquid comes into proximity with the heated region.

The importance of maintaining the liquid hydrogen in a cool state to the region where the heat transfer is expected is demonstrated in Fig. 12. The parameter varied between the flows resulting in the interface temperatures shown was the inlet temperature. Understandably the interface temperatures are much larger for higher inlet temperatures, though the demonstrated rise in temperature maximums may seem disproportionately large compared to the increased inlet temperatures. However, the fluid densities are twice that at 55 K (63 kg/m³) as at 155 K (26 kg/m³). For the very lowest temperatures, a higher maximum temperature was observed for an inlet temperature of 26 K than for an inlet temperature of 55 K. This occurred because of the influence of the different states of the hydrogen at these two temperatures. At 26 K the hydrogen behaves like a viscous liquid, while at 55 K its density is lower, and therefore, boundary-layer development is slower.

The ability of the coolant to cool the structure sufficiently is dependent on the velocity of the coolant. Figure 13 shows the interface temperature for a range of fluid velocities under otherwise baseline conditions. These velocities correspond to Reynolds numbers (based on the inlet height and inlet fluid properties) of between $0.28 \times 10^6 \times 2.27 \times 10^6$. Figure 14 shows the temperatures resulting from the same range of velocities for a lower inlet pressure, corresponding to inlet Reynolds numbers from 0.34×10^6 to 2.70×10^6.

To confirm that the effects observed, e.g., the relationship of the maximum temperature with inlet temperature, were not merely due to the decreased mass flow rate resulting from the decreased density at the lower temperature, a series of cases were run for the same total mass flow rate but different inlet conditions. Figure 15 shows the interface temperatures for these cases. The results confirm the large influence on outlet temperature of inlet temperature, even with mass flow rate and pressure maintained, and the similar effects of de-

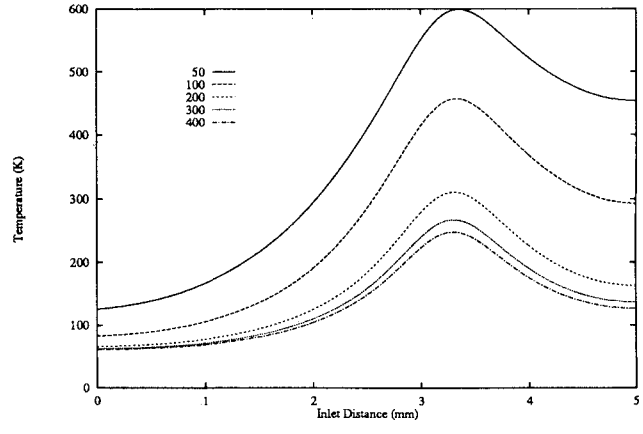

Fig. 13 Interface temperatures for a range of inlet velocities, given in m/s.

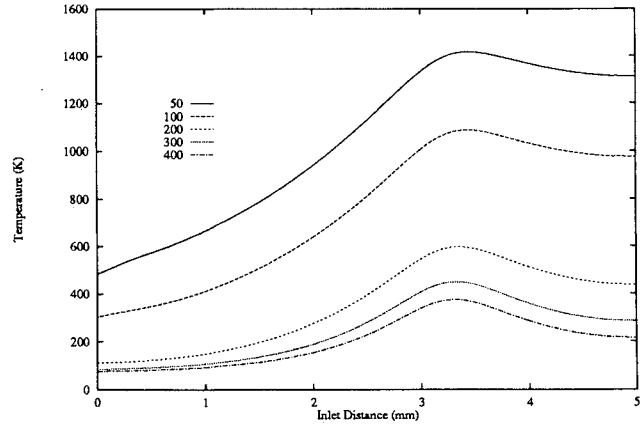

Fig. 14 Interface temperatures for a range of inlet velocities, given in m/s, for an inlet pressure of 5 MPa.

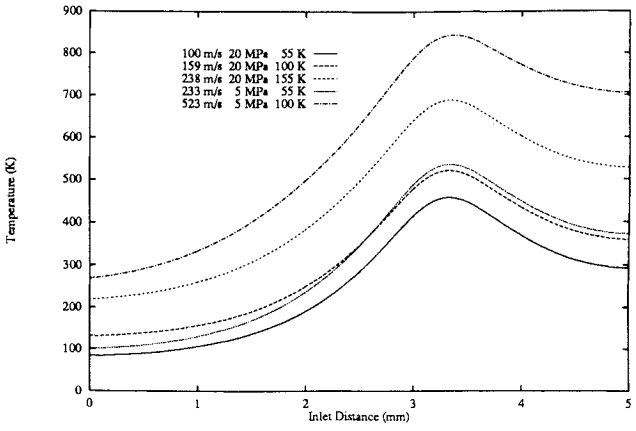

Fig. 15 Interface temperatures for a range of inlet conditions, maintaining the same mass flow rate.

creases in fluid pressure with the other factors maintained constant. It is interesting to see that, for the same mass flow rate, the change in maximum temperature caused by an increase in inlet temperature of 45 K and a constant pressure, is similar to that caused by a reduction of the pressure to a quarter of its previous value and a constant inlet temperature.

IV. Conclusions

An algorithm based on the two-dimensional parabolized Navier-Stokes equations was implemented. It solved the coupled problems of the heat transfer from an externally heated solid region to an internal coolant fluid, allowing for variation of thermophysical properties of the fluid with temperature. The variations in the fluid properties were modeled by matching polynomials to the known properties of liquid hydrogen, and the turbulence shear stresses and thermal diffusivity were modeled by a mixing length theory. It was found that the interface between the solid and the fluid was most efficiently treated by considering the interface temperature as the boundary condition in the fluid, and the local heat transfer coefficient as the boundary condition for the solid. The algorithm was applied to the application of the massive heating generated by the external aerodynamic flow over the engine cowl lip of the NASP which is internally cooled by liquid hydrogen.

The conclusions to the parametric study of the factors influencing the heat transfer capabilities of this system are that, for the baseline configuration, the temperature rises are excessive (maximum temperature ~700 K). The temperatures are completely dependent on the incident heat load which has been assumed to be a loading of 500 MJ/m^{2}s over a width of 0.25 mm. If either the width of the external phenomenon or the area heat transfer rate is significantly larger, the capability of the hydrogen coolant to transfer the heat will be exceeded. Other parametric studies showed that there is little influence on maximum temperatures of an increase of inlet temperature from 25 to 55 K, but that maximum temperatures increase rapidly for inlet temperatures above that. Also, the beneficial effects of higher coolant velocities and higher fluid pressures were demonstrated.

References

[1]Korkegi, R. H., "Survey of Viscous Interactions Associated with High Mach Number Flight," *AIAA Journal*, Vol. 9, May 1971, pp. 771–784.

[2]Edney, B. E., "Effects of Shock Impingement on the Heat Transfer Around Blunt Bodies," *AIAA Journal*, Vol. 6, Jan. 1968, pp. 15–21.

[3]Scotti, S. J., "Numerical Studies of Convective Cooling for Locally Heated Skin," NASA Langley Research Center, TP 3100, Hampton, VA, May 1991.

[4]Holden, M. S., Wieting, A. R., Moselle, J. R., and Glass, C., "Studies of Aerothermal Loads Generated in Regions of Shock/Shock Interaction in Hypersonic Flow," AIAA Paper 88-0477, Jan. 1988.

[5]Bauer, P. E., and Collicott, H. E., *Entry Vehicle Heating and Thermal Protection Systems: Space Shuttle, Solar Starprobe, Jupiter Galileo Project*, edited by M. Summerfield, Vol. 85, Progress in Astronautics and Aeronautics, AIAA, New York, 1983.

[6]Edney, B., "Anomalous Heat Transfer and Pressure Distributions on Blunt Bodies at Hypersonic Speeds in the Presence of Impinging Shocks," Aeronautical Research Inst. of Sweden, Rept. 115, Stockholm, Sweden, Feb. 1968.

[7]Dziedzic, W. M., Jones, S. C., Gould, D. C., and Petley, D. H., "An Analytic Comparison of Convective Heat Transfer Correlations in Supercritical Hydrogen," AIAA Paper 91-1382, June 1991.

[8]Taylor, M. F., "Correlation of Local Heat-Transfer Coefficients for Single-Phase Turbulent Flow of Hydrogen in Tubes with Temperature Ratios to 23," NASA TN D-4332, Jan. 1968.

[9]Buelow, P. E., Tannehill, J. C., Ievalts, J. O., and Lawrence, S. L., "Three-Dimensional, Upwind, Parabolized Navier-Stokes Code for Chemically Reacting Flows," *Journal of Thermophysics and Heat Transfer*, Vol. 5, No. 3, 1991, pp. 274–283.

[10]Chyou, Y. P., "The Effect of a Short Unheated Length and a Concentrated Heat Source on the Heat Transfer Through a Turbulent Boundary Layer," *International Journal of Heat and Mass Transfer*, Vol. 34, No. 8, 1991, pp. 1917–1928.

[11]Guedes, R. O. C., Cotta, R. M., and Brum, N. C. L., "Heat Transfer in Laminar Flow with Axial Conduction and External Convection," *Journal of Thermophysics and Heat Transfer*, Vol. 5, No. 4, 1991, pp. 508–513.

[12]Cebeci, T., and Bradshaw, P., *Physical and Computational Aspects of Convective Heat Transfer*, 1st ed., Springer-Verlag, New York, 1984.

[13]Fletcher, C. A. J., *Computational Techniques for Fluid Dynamics*, 1st ed., Springer-Verlag, Berlin, 1988, pp. 280, 281.

[14]Carlisle, R. G., "Computational Modeling of Convective Heat Transfer to Liquid Hydrogen Coolant," Ph.D. Dissertation, Univ. of Virginia, Charlottesville, VA, Aug. 1992.

[15]McCarty, R. D., Hord, J., and Roder, H. M., "Selected Properties of Hydrogen (Engineering Design Data)," NBS Monograph 168, National Bureau of Standards, Washington, DC, 1981.

[16]Saladino, A., and Praharaj, S., "PARCEQ2D Heat Transfer Grid Sensitivity Analysis," AIAA 29th Aerospace Sciences Meeting, Reno, NV, Jan. 1991.

[17]Thompson, J. F., Warsi, Z. U. A., and Mastin, C. W., *Numerical Grid Generation: Foundations and Applications*, North-Holland, New York, 1985.

[18]Hess, H. L., and Kunz, H. R., "A Study of Forced Convection Heat Transfer to Supercritical Hydrogen," *Journal of Heat Transfer*, Vol. 87, No. 1, 1965, pp. 41–48.

[19]McCarthy, J. R., and Wolf, H., "The Heat Transfer Characteristics of Gaseous Hydrogen and Helium," Rocketdyne Div., TR R-60-12, North American Aviation, Anaheim, CA, Dec. 1960.

[20]Miller, W. S., Seader, J. D., and Trebes, D. M., "Forced Convection to Liquid Hydrogen at Super-Critical Pressures," *Pure and Applied Cryogenics*, Vol. 4, 1965, Sec. IV, pp. 173–191.